A Multi-omic approach reveals iron availability influences hepatocyte cell fate

Athena Jessica S Ong[1,2], Tara A Tigani[1,2], Jordyn M Reinecke[1], Andrew G Cox[1,2,3*], and Kristin K Brown[1,2,3*]

[1]Peter MacCallum Cancer Centre, Melbourne, Victoria, 3000, Australia
[2]The Sir Peter MacCallum Department of Oncology, The University of Melbourne, Melbourne, Victoria, 3010, Australia
[3]Department of Biochemistry and Pharmacology, The University of Melbourne, Melbourne, Victoria, 3010, Australia

*Equal contribution
Corresponding authors: kristin.brown@petermac.org, andrew.cox@petermac.org

Abstract

Recent evidence has highlighted the importance of employing cell culture media designed to reproduce the physiological metabolic environment *in vitro*. Here, we utilize the physiological medium Plasmax to examine the impact of nutrient availability on the model human hepatocyte cell line, HepG2. Incubation of HepG2 cells in Plasmax suppressed a transcriptional program driven by Hepatocyte Nuclear Factor 4 (HNF4A), a master regulator of hepatocyte identity. Given that HepG2 cells were originally isolated from a patient with hepatoblastoma, this suggests reversion to the native state in physiological media. Importantly, exclusion of the trace element iron from Plasmax reinstated the HNF4A-driven transcriptional program. Taken together, these studies suggest a relationship between iron availability and regulation of hepatocyte cell fate and highlight the importance of more faithfully recapitulating *in vivo* metabolite availability *in vitro*.

Introduction

In vitro cell culture models play a central role in biological and biomedical research. In recent years, efforts to improve the physiological relevance of these models have highlighted the importance of media composition on cellular phenotype and biological responses (Lagziel *et al*, 2020; Vande Voorde *et al*, 01/2019; Cantor *et al*, 2017; Rossiter *et al*, 2021; Senkowski *et al*, 2023). For example, the dependence of some cancer cell lines on glutaminolysis is not observed in the *in vivo* context (Davidson *et al*, 2016). This has been attributed to the presence of high cystine concentrations in conventional *in vitro* culture conditions (Muir *et al*, 2017). More generally, conventional media (e.g. Dulbecco's Modified Eagle's Medium, DMEM) poorly recapitulate metabolite levels that cells would be exposed to *in vivo* (Eagle, 1959; Dulbecco & Freeman, 1959). The increasing awareness and recognition that the composition of cell culture media is important in preserving biological processes *in vitro* has led to ongoing efforts to develop cell culture media that better represent physiological metabolite concentrations (Vande Voorde *et al*, 2019; Cantor *et al*, 2017; Muir & Vander Heiden, 2018; Tardito *et al*, 2015; Cantor, 2019). These studies have demonstrated that cell culture media composition can alter cellular dependencies via metabolic and transcriptional changes (Davidson *et al*, 2016; Biancur *et al*, 2017; Flickinger *et al*, 2024; Vande Voorde *et al*, 2019; Cantor *et al*, 2017; Apiz Saab *et al*, 2023; Rawat *et al*, 2024).

Hepatocytes, the major cell type in the liver, are widely modelled *in vitro* to study drug metabolism, drug-induced liver injury (DILI), and various liver diseases (Kaur *et al*, 2023; Yang *et al*, 2023). The most commonly used cell line in these contexts are HepG2 cells (Arzumanian *et al*, 2021). HepG2s were originally derived from a hepatic tumour isolated from a 15-year-old male (Aden *et al*, 1979). Although initially characterised as being derived from a hepatocellular carcinoma (HCC), subsequent histopathologic, genetic and molecular analysis revealed that the origin of HepG2 cells was instead a hepatoblastoma (HB) (López-Terrada *et al*, 2009). Despite this, HepG2 cells are still widely utilized as a hepatocyte cell line as they exhibit the hallmarks of hepatocyte fate and function *in vitro* (Liu *et al*, 2022, 2021; Lin *et al*, 2016; Park *et al*, 2018; Zhang *et al*, 2018).

In this study, we examined the impact of nutrient availability on HepG2 cells by comparing culture in conventional media with culture in a media previously developed to more faithfully reflect metabolite abundance in human plasma (Plasmax) (Vande Voorde *et al*, 2019). We demonstrate that culturing HepG2 cells in Plasmax alters cell fate in a manner associated with loss of HNF4A, the master transcriptional regulator of hepatic gene expression. Mechanistically, we demonstrate that iron availability contributes to the regulation of hepatic cell fate. This research suggests an important role for physiological media in maintaining cell fate *in vitro*.

Results

HepG2 cells adopt a native hepatoblast-like state in physiological media

Typically, HepG2 cells are maintained in one of three conventional cell culture media: EMEM, high glucose DMEM (HG-DMEM) or low glucose DMEM (LG-DMEM) (Sanghvi *et al*, 2019; Chen *et al*, 2024; Jiang *et al*, 2023; Ong *et al*, 2023). To examine the impact of culture media on the transcriptional landscape, HepG2 cells were cultured in each of the three conventional media types or in the physiological medium Plasmax (Vande Voorde *et al*, 2019). Plasmax mimics metabolite concentrations found in human plasma and has a dramatically different composition than conventional cell culture media (Fig. S1A). While minimal transcriptional changes were observed in response to culture in any of the three conventional media, culture in Plasmax induced widespread transcriptional changes (Fig. S1B,C). Amongst the most significant changes observed in Plasmax, relative to EMEM, was upregulation of the pioneer transcription factor SRY-Box Transcription Factor 4 (*SOX4*), a regulator of hepatocyte dedifferentiation, and concomitant downregulation of genes (Apolipoprotein H, *APOH*; Albumin, *ALB*; Transferrin, *TF*) controlled by Hepatocyte Nuclear Factor 4 Alpha (HNF4A), a transcription factor that regulates hepatocyte identity (Fig. 1A) (Parviz *et al*, 2003; Sekiya & Suzuki, 2011; Katsuda *et al*, 2024). Downregulation of HNF4A in Plasmax was confirmed at the level of protein expression (Fig. 1B). Consistent with these observations, Gene Set Enrichment Analysis (GSEA) revealed downregulation of signatures associated with hepatocyte cell state and hepatocyte function in the context of culture in Plasmax (Fig. 1C). In the developmental context, hepatoblasts are bipotential progenitor cells that differentiate to give rise to both hepatocytes and cholangiocytes (Fig. S1D)(Gordillo *et al*, 2015). Culture in Plasmax induced an increase in the expression of genes associated with a hepatoblast-like state (e.g. Epithelial Cell Adhesion Molecule, *EPCAM* and SRY-Box Transcription Factor 9, *SOX9*) and, as previously mentioned, loss of genes associated with differentiated hepatocytes (e.g. *ALB*, *APOH*, and *TF*) suggesting that culture in physiological media drives dedifferentiation (Fig. 1D). Interestingly, analysis of a publicly available dataset examining the impact of culture conditions on the basal-like breast cancer cell line MDA-MB-468 revealed a shift to a progenitor-like state when cells were cultured in Plasmax (Fig. S1E) (Vande Voorde *et al*, 2019; Charafe-Jauffret *et al*, 2006; Neve *et al*, 2006).

Trace element availability regulates hepatocyte differentiation

To examine the components of Plasmax contributing to dedifferentiation of HepG2 cells, variants of Plasmax lacking either trace elements, which are severely underrepresented in EMEM/DMEM, or lacking metabolites absent from EMEM/DMEM (termed “supplemental metabolites”) were prepared (Fig. S1A) (Vande Voorde *et al*, 2019). Withdrawal of trace elements, but not supplemental metabolites, restored HNF4A protein expression to levels

104 observed in EMEM (Fig. 2A). Moreover, transcriptomics revealed that trace element
105 withdrawal restored hepatocyte gene expression and expression of signatures associated with
106 hepatocyte cell state and hepatocyte function (Fig. 2B,C). Notably, *SOX4* expression was
107 suppressed and returned to levels observed in EMEM when cells were cultured in Plasmax
108 devoid of trace elements (Fig. 2C,D).
109
110 **Multi-omics analysis reveals a relationship between trace element availability and**
111 **metalloprotein expression**
112 In order to gain insights regarding which trace element(s) was contributing to
113 dedifferentiation in Plasmax, intracellular trace element abundance was quantified using
114 inductively-coupled plasma mass spectrometry (ICP-MS). Given that serum can be a source
115 of trace elements, trace elements were also quantified in fresh culture media. As expected,
116 trace elements were elevated in Plasmax compared to EMEM (Fig. S2A). Interestingly, despite
117 iron levels being increased by only four-fold in Plasmax relative to EMEM, HepG2 cells
118 cultured in Plasmax exhibited more than a twenty-fold increase in intracellular iron (Fig. 3A).
119 A three-fold increase in intracellular copper was also observed (Fig. 3A). To explore the role
120 of iron in hepatocyte differentiation, iron salts were added back to Plasmax devoid of trace
121 elements. A multidimensional scaling (MDS) plot of the transcriptome revealed that while
122 withdrawal of trace elements from Plasmax resulted in a transcriptome more similar to EMEM,
123 reintroduction of iron resulted in a transcriptome that was more similar to Plasmax (Fig. 3B).
124 This trend was recapitulated at the proteome level where reintroduction of iron restored a
125 proteomic profile similar to HepG2 cells incubated in complete Plasmax (Fig. 3C). Interestingly,
126 a correlation plot of the transcriptome and proteome of cells cultured in Plasmax lacking trace
127 elements compared to complete Plasmax revealed proteins that were significantly
128 downregulated at the protein, but not the transcript, level in response to removal of trace
129 elements. Notably, among these proteins were selenoproteins (e.g. Selenoprotein P,
130 *SELENOP* and Glutathione Peroxidase 1, *GPX1*) and iron-regulated proteins (e.g. Ferritin
131 Heavy Chain 1, *FTH1*) (Fig. 3D). These proteins belong to the metalloprotein superfamily and
132 their translation is dependent on trace element availability (Copeland, 2003; Addess *et al*,
133 1997). Consistent with this, addition of iron salts to Plasmax devoid of trace elements was
134 able to rescue the expression of iron-regulated proteins but not selenoproteins, demonstrating
135 the importance of trace elements in the post-transcriptional regulation of protein abundance
136 (Fig. 3E). Taken together, these results highlight a role for trace elements in the regulation of
137 cellular phenotype and demonstrate the importance of utilizing a multi-omic approach to
138 interrogate the impact of altered nutrient availability.
139
140 **Iron availability contributes to the regulation of hepatocyte cell fate**

141 Given that the intracellular levels of iron and copper were significantly increased in
142 HepG2 cells cultured in Plasmax (Fig. 3A), these trace elements were further examined for
143 their role in modulating hepatocyte cell fate. Interestingly, reintroduction of iron salts, but not
144 copper salts, to Plasmax devoid of trace elements suppressed HNF4A expression (Fig. 4A).
145 Moreover, re-introduction of iron salts suppressed signatures associated with the differentiated
146 hepatocyte cell state (Fig. 4B,C). The majority of labile iron is incorporated in the cofactor
147 heme(Ajioka *et al*, 2006). The transcriptional repressor BTB and CNC Homolog 1 (BACH1)
148 plays a central role in regulating intracellular heme homeostasis and is itself regulated by
149 heme availability (Oyake *et al*, 1996; Ogawa *et al*, 2001; Sun *et al*, 2002). Interestingly, BACH1
150 has also been shown to contribute to the regulation of cell fate (Wei *et al*, 03 2019; Oyake *et*
151 *al*, 1996). Notably, proteomics analysis revealed that BACH1 target genes were upregulated
152 after reintroduction of iron salts to Plasmax devoid of trace elements (Fig. 4D). Finally, BACH1
153 protein expression was dramatically lower in HepG2 cells cultured in Plasmax versus EMEM
154 (Fig. 4E). Taken together, these data suggest that the iron-dependent dedifferentiation of
155 hepatocytes in Plasmax is mediated by the trace element iron through regulation of the
156 transcription factor BACH1 (Fig. S3A).
157
158 **Discussion**
159 The liver biopsy from which HepG2 cells were isolated in 1979 was described as a well
160 differentiated HCC (Aden *et al*, 1979). It was not until 2009 when the histopathology and
161 genetics of the original biopsy was revisited that it was reclassified as a HB (López-Terrada *et*
162 *al*, 2009). Despite this correction, HepG2 cells are still widely used to model hepatocytes/HCC
163 rather than hepatoblasts/HB (Liu *et al*, 2022, 2021; Lin *et al*, 2016; Park *et al*, 2018; Zhang *et*
164 *al*, 2018). This is reasonable as HepG2 cells cultured in conventional media exhibit
165 characteristics consistent with differentiated hepatocytes (Fig. 1C). In this study, we have
166 demonstrated that incubation in a physiological medium, Plasmax, causes HepG2 cells to
167 revert to their native hepatoblast state.
168 A previous study investigating the impact of cell culture conditions on HepG2 cells
169 demonstrated that increased amino acid availability promoted the acquisition of a
170 transcriptome similar to primary human hepatocytes (Boon *et al*, 12/2020). In other cell lines,
171 physiologically relevant metabolites that are underrepresented or absent in conventional
172 media, such as urea and the trace element selenium, have been shown to drive significant
173 changes in cell metabolism (Cantor *et al*, 2017; Vande Voorde *et al*, 2019). Here, we have
174 shown that underrepresentation of the trace element iron in conventional media drives
175 differentiation of HepG2 cells to a hepatocyte state. Maintenance of intracellular iron
176 homeostasis has been shown to play a role in determining fate in other cell types including
177 breast cancer cells, hematopoietic stem cells and alveolar cells (Kao *et al*, 2024; Zhuang *et*

178 *al*, 2025; Müller *et al*, 2020). Although trace elements exist in minute quantities in the plasma,
179 these studies highlight the importance of considering trace element availability when
180 employing cell culture models.

181 We demonstrate that removal of trace elements from Plasmax triggers the
182 downregulation of proteins harbouring iron response elements in the 5'-UTR of the associated
183 transcripts (IRE; e.g. ACO2, FTL, FTH1) (Aziz & Munro, 1987; Hentze *et al*, 1987; Shen *et al*,
184 2023). IREs are recognized by IRE binding proteins, which in the absence of iron, repress
185 protein expression by hindering the binding of translation initiation factors (Gray & Hentze,
186 1994). In addition to iron, the availability of other trace elements can dramatically impact the
187 proteome. For example, the translation of selenoproteins, which contain the cysteine analogue
188 selenocysteine (Sec), is dependent on selenium availability (Zinoni *et al*, 1986; Chambers *et*
189 *al*, 1986; Copeland, 2003; Kryukov *et al*, 2003). Since the protein expression of IRE-containing
190 proteins and selenoproteins are regulated at the translational level, changes in their
191 expression resulting from altered trace element availability would not be detected at the
192 transcriptional level. This underscores the importance of employing multi-omic approaches to
193 investigate the consequences of altering metabolite availability.

194 BACH1 is a transcription factor that regulates iron homeostasis and is highly
195 responsive to changes in iron availability (Kitamuro *et al*, 2003; Chen *et al*, 2023). Interestingly,
196 in lung cancer, BACH1 has been shown to drive changes in cell plasticity via epithelial-to-
197 mesenchymal transition (Wiel *et al*, 2019; Lignitto *et al*, 2019). Moreover, BACH1 has been
198 shown to interact with transcription factors that regulate self-renewal (e.g. NANOG, SOX2,
199 and OCT4) to repress transcription of mesodermal genes and promote pluripotency in human
200 embryonic stem cells (Wei *et al*, 2019). Our findings demonstrate that BACH1 is
201 downregulated in HepG2 cells cultured in Plasmax (Fig. 4E). Future studies investigating the
202 interplay between iron availability, BACH1 and cell fate are warranted.

203 In conclusion, our study adds to a growing body of literature highlighting the importance
204 of more faithfully recapitulating the *in vivo* metabolic microenvironment when employing *in*
205 *vitro* cell culture models. In light of these findings, we suggest that, in addition to providing an
206 opportunity to identify novel modulators of cell fate, physiological media will improve the *in*
207 *vivo* relevance of *in vitro* cell culture models.

208

209

210 **Materials and Methods**

211 **Cell culture**

212 HepG2 cells were purchased from the European Collection of Authenticated Cell Cultures
213 (ECACC) via CellBank Australia (85011430) and were routinely assayed for mycoplasma
214 contamination. HepG2 cells were cultured in high glucose DMEM (DMEM-HG; Thermo Fisher

215 Scientific, 11965118), low glucose DMEM (DMEM-LG; Thermo Fisher Scientific, 11885084),
216 Plasmax (prepared in-house as previously described (Vande Voorde *et al*, 2019)) or EMEM,
217 which was prepared by supplementing MEM, NEAA, no glutamine (Thermo Fisher Scientific,
218 10370) with 1 mM sodium pyruvate, 2 mM glutamine. HepG2 cells were maintained in a
219 humidified incubator at 37°C with 5% CO_2. For all experiments, $2x10^5$ HepG2 cells were
220 seeded in 6-well plates in EMEM containing 10% heat-inactivated FBS (HyClone™,
221 SH30084). 24 hours after seeding, wells were washed with PBS and the appropriate media
222 (DMEM-HG, DMEM-LG, Plasmax or EMEM) containing 10% heat-inactivated FBS was
223 added. Media was refreshed after 48 hours and cells were harvested 96 hours after transition
224 to the different media types.
225
226 **RNA-Seq analysis**
227 For RNA-Seq analysis, total RNA was extracted using the NucleoSpin RNA kit (Macherey-
228 Nagel, 740955) as per manufacturer's instructions. RNA quality was confirmed using an
229 Agilent 4200 TapeStation System. Libraries were prepared using the QuantSeq 3' mRNA-Seq
230 kit (Lexogen, 015) and sequenced with an Illumina NextSeq 500, with single-end 75 bp reads
231 to a depth of 5 M reads per sample. FASTQ files were uploaded to the Galaxy web platform
232 for quality control (FastQC), trimming (Cutadapt), alignment (RNA STAR), and counting
233 (featureCounts) (Afgan *et al*, 2016). Reads were aligned to the human genome assembly
234 (Ensembl hg19, GRCh37). Analysis of differentially expressed genes was performed with
235 Limma-Voom (v3.40.6) (Smyth, 2005; Law *et al*, 2014). Gene set enrichment analysis (GSEA)
236 was performed and plotted in R using the 'clusterProfiler' package (Yu *et al*, 2012). Heatmaps
237 and volcano plots were generated in R using the 'pheatmap' and 'ggplot' packages
238 respectively(Kolde, 2012; Wickham, 2016).
239
240 **Quantitative polymerase chain reaction (qPCR)**
241 Total RNA was isolated using the NucleoSpin RNA Kit (Macherey-Nagel, 740955) following
242 manufacturer's instructions. Complementary DNA (cDNA) was synthesized using the High-
243 Capacity cDNA Reverse Transcription Kit (Thermo Fisher Scientific, 4368813) according to
244 the manufacturer's guidelines. cDNA was diluted 5-fold in nuclease-free H_2O (Thermo Fisher
245 Scientific, 10977015). qPCR was performed using Applied Bioystems Fast SYBR™ Green
246 Master Mix (Thermo Fisher Scientific, 4385616) and the Applied StepOnePlus Real-Time PCR
247 System (Thermo Fisher Scientific). Primers for *RPLP0* (5'-CAGATTGGCTACCCAACTGTT-3'
248 and 5'-GGGAAGGTGTAATCCGTCTCC-3'), *ALB* (5'-CTTGAATGTGCTGATGACAGG-3' and
249 5'-GCAAGTCAGCAGGCATCTCAT-3'), and *ACAT2* (5'-GCGGACCATCATAGGTTCCTT-3'
250 and 5'- CTGCAAGGCACACAGCTTTT-3') were used for qPCR. Relative gene expression was
251 determined using the ΔΔCt method(Rao *et al*, 2013) normalised to *RPLP0*.

252

253 **Immunoblotting**

254 Cells were washed with PBS and lysed in SDS lysis buffer (1% SDS, 50 mM Tris-HCl, 10 mM
255 EDTA) containing a protease inhibitor cocktail (Sigma-Aldrich, P8340) and Pierce™ Universal
256 Nuclease for Cell Lysis (Thermo Fisher Scientific, 88072). Lysates were resolved by SDS-
257 PAGE and transferred to nitrocellulose membrane. Membranes were probed with primary
258 antibodies recognising HNF4A (Cell Signaling Technology, 3113, 1:1000 dilution), BACH1
259 (Proteintech, 14018-1-AP, 1:500 dilution), and β-Actin (Cell Signalling Technology, 3700,
260 1:5000 dilution). Membranes were incubated with IRDye secondary antibodies (LI-COR, 926-
261 68070 and 926-32211) and imaged using the Odyssey DLx imaging system (LI-COR).

262

263 **Inductively-coupled plasma mass spectrometry (ICP-MS)**

264 ICP-MS was performed as previously described(Pyun *et al*, 2022). Cells were washed with
265 PBS and whole cell lysates were collected in SDS lysis buffer. Media with 10% FBS (500 µL)
266 was used to determine trace element abundance in EMEM and Plasmax. Lysates or media
267 were lyophilized prior to digestion in 65% nitric acid (Merck, 100441). Samples were heated
268 at 90˚C for 20 minutes to complete the digestion and subsequently diluted with 1% (v/v) nitric
269 acid. Samples were run on the Agilent 8800 (ICPMS-QQQ-8800) system using a Helium
270 reaction gas cell. Raw parts per billion (ppb) data of the elements were converted to µmol/L
271 with dilution factors applied. The final concentrations of the metals were corrected with the
272 treatment blanks and normalized to the total protein to obtain a final unit expressed as
273 metal/mg protein. Fold changes were normalized to the average of controls.

274

275 **Proteomic Analysis**

276 Cells were washed with PBS and lysed in 200 µL of ice-cold RIPA buffer (1% NP-40, 0.5%
277 sodium deoxycholate, 0.1% SDS, 150 mM NaCl, 50 mM Tris-HCl, pH 7.5) containing a
278 protease-inhibitor cocktail (Sigma-Aldrich, P8340) and phosphatase inhibitors (Roche,
279 4906845001). Protein (50 µg per sample) was reduced by adding a final concentration of 10
280 mM TCEP (Sigma-Aldrich, 646547) and incubated at 37˚C for 45 min. Samples were then
281 alkylated with 50 mM iodoacetamide (Sigma-Aldrich, I1149) and incubated in the dark for 45
282 min. After acidification with 2.5% phosphoric acid (Sigma-Aldrich, 79617), samples were
283 passed through S-Trap micro columns (Protifi, C02-micro). Proteins were digested overnight
284 at 37˚C with a 1:20 dilution of Pierce™ Trypsin Protease (Thermo Fisher Scientific, 90057).
285 Peptides were eluted sequentially with 50 mM triethylammonium bicarbonate buffer (TEAB),
286 0.2% formic acid, and 50% acetonitrile/0.2% formic acid. Finally, the eluent was lyophilized
287 and reconstituted in 2% acetonitrile/0.05% trifluoroacetic acid to make up the peptide solution
288 for LC-MS/MS analysis by data-independent acquisition using a Thermo OrbiTrap Ascend

289 mass spectrometer. Data analysis was performed using the software suite, DIA-NN (Demichev
290 *et al*, 2020). Heatmaps and volcano plots were generated in R using the 'pheatmap' and
291 'ggplot' packages respectively (Kolde, 2012; Wickham, 2016).
292
293 **Quantification and Statistical Analysis**
294 Statistical analyses were performed with Prism 9 software (GraphPad Software). All statistical
295 analyses for data comparing two groups were performed with an unpaired Student's t-test.
296 One-way ANOVA with the Holm–Sidak method for multiple comparisons was used for
297 comparison of more than two groups. All immunoblots are representative of results from at
298 least three independent experiments. All other statistical details of experiments can be found
299 in the figure legends.
300
301 **Acknowledgements**
302 A.J.S.O. is supported by a Peter MacCallum Cancer Centre Foundation Grant. T.A.T. is
303 supported by an Australian Government Research Training Program Scholarship. K.K.B. is
304 supported by NHMRC Ideas Grants (GNT2004212 and GNT2012313) and a Victorian Cancer
305 Agency Mid-Career Research Fellowship (MCRF17020). A.G.C. is supported by a National
306 Health and Medical Research Council (NHMRC) Investigator Grant (GNT1176650), and an
307 Australian Research Council Discovery Project Grant (DP200102693). K.K.B and A.G.C. are
308 also jointly supported by the Peter MacCallum Cancer Foundation (Ted and Lila Seehusen
309 Foundation). We acknowledge support from the Peter MacCallum Cancer Centre Foundation
310 and the Australian Cancer Research Foundation. We acknowledge the Bio21 Melbourne Mass
311 Spectrometry and Proteomics Facility (MMSPF) at the University of Melbourne and the
312 Biometals Facility at the Florey Institute of Neuroscience and Mental Health (University of
313 Melbourne) for their training, support, and technical assistance. We extend our thanks to the
314 Peter MacCallum Cancer Centre Core Facilities and their staff who provided support for this
315 work; namely the Molecular Genomics Core, the Flow Cytometry Core and the Bioinformatics
316 Core Facilities. Finally, we thank members of the Cox Laboratory and Brown Laboratory (Peter
317 MacCallum Cancer Centre) for helpful discussions.
318
319 **Author contributions**
320 A.J.S.O., A.G.C., and K.K.B. designed research; A.J.S.O., T.A.T., and J.M.R. performed
321 research; A.J.S.O. analyzed data; A.G.C. and K.K.B. supervision; and A.J.S.O., A.G.C., and
322 K.K.B. wrote the paper.

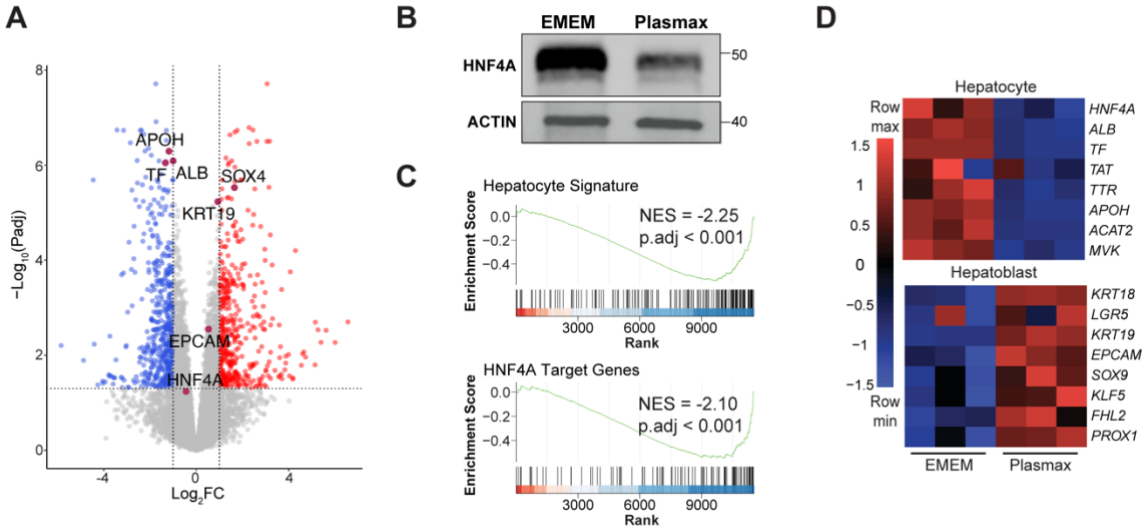

Figure 1. HepG2 cells adopt a native hepatoblast-like state in physiological media. (A) Volcano plot of differentially expressed genes (DEGs) identified from RNA-Seq analysis comparing HepG2 cells cultured in Plasmax with HepG2 cells cultured in EMEM, n=3. Hepatocyte differentiation markers are highlighted in maroon. Significantly upregulated genes are highlighted in red. Significantly downregulated genes are highlighted in blue. (B) Representative immunoblot analysis of HepG2 cells cultured in EMEM or Plasmax. (C) Gene set enrichment analysis (GSEA) plots derived from RNA-Seq analysis comparing HepG2 cells cultured in Plasmax with HepG2 cells cultured in EMEM demonstrating signatures associated with hepatocyte cell state and function. (D) Heatmap of hepatocyte and hepatoblast gene expression in HepG2 cells culture in EMEM or Plasmax as determined by RNA-Seq analysis, n=3.

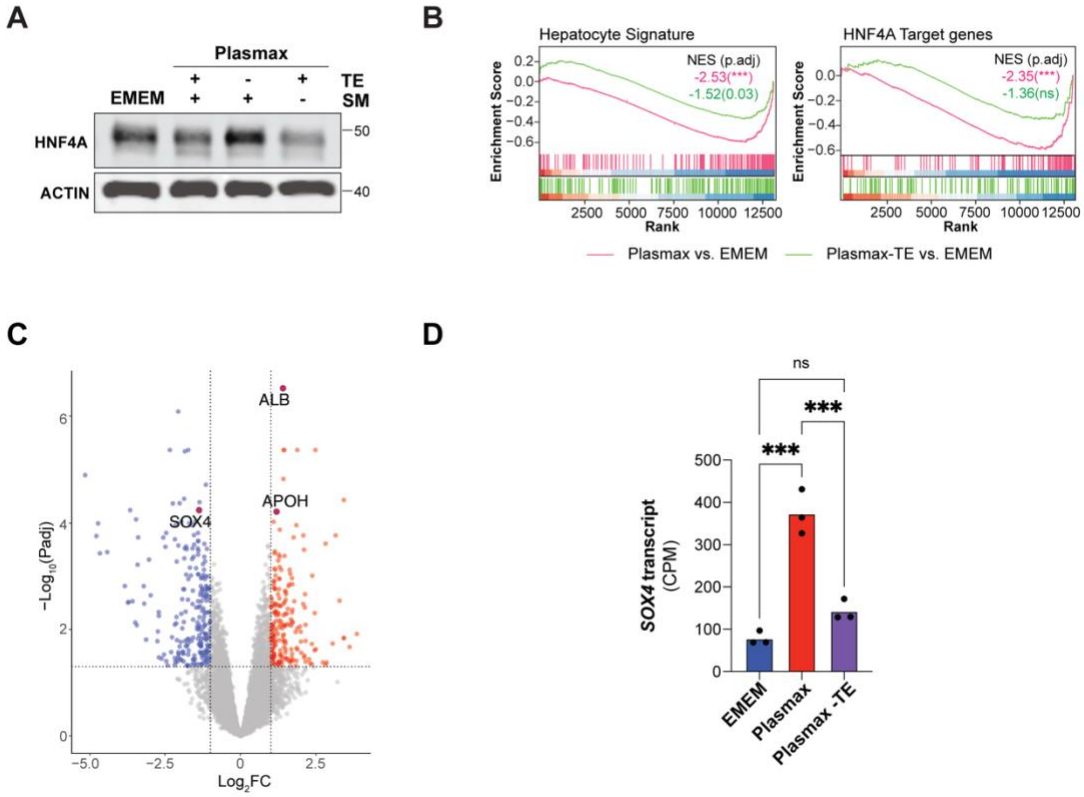

Figure 2. Trace element availability regulates hepatocyte differentiation
(A) Representative immunoblot analysis of HepG2 cells cultured in EMEM, Plasmax, Plasmax devoid of trace elements (TE) or Plasmax devoid of supplemental metabolites (SM). (B) GSEA plots derived from RNA-Seq analysis comparing HepG2 cells cultured in Plasmax with HepG2 cells cultured in EMEM or comparing HepG2 cells cultured in Plasmax-TE with HepG2 cells cultured in EMEM demonstrating signatures associated with hepatocyte cell state and function. (C) Volcano plot of DEGs identified from RNA-Seq analysis comparing HepG2 cells cultured in Plasmax-TE with HepG2 cells cultured in Plasmax, n=3. Hepatocyte differentiation markers are highlighted in maroon. Significantly upregulated genes are highlighted in red. Significantly downregulated genes are highlighted in blue. (D) *SOX4* transcript expression in counts per million (CPM) based on RNA-Seq analysis of HepG2 cells cultured in EMEM, Plasmax, or Plasmax-TE, n=3. For all experiments, ***P <0.001, ns = not significant.

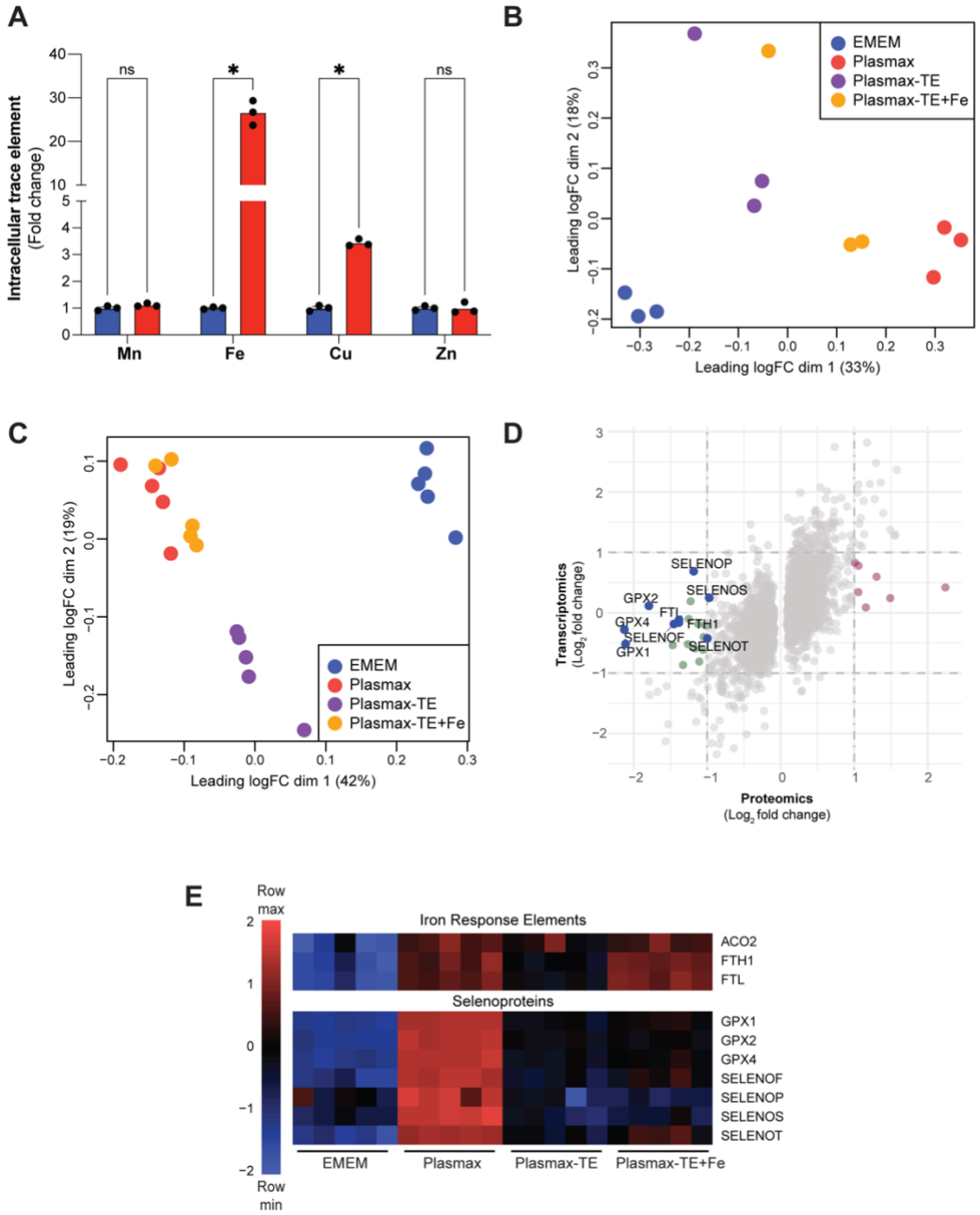

Figure 3. Multi-omics analysis reveals a relationship between trace element availability and metalloprotein expression

(A) Relative intracellular abundance of trace elements in HepG2 cells cultured in EMEM (blue) or Plasmax (red) n=3. (B) MDS plot of RNA-Seq data from HepG2 cells cultured in EMEM, Plasmax, Plasmax-TE, or Plasmax-TE supplemented with iron salts (0.12 μM ferric nitrate and 1.04 μM ferric sulfate; Plasmax-TE+Fe), n=3. (C) MDS plot of proteomic data from HepG2 cells cultured in EMEM, Plasmax, Plasmax-TE, or Plasmax-TE+Fe, n=5. (D) Correlation between proteomic and transcriptomic data from HepG2 cells cultured in Plasmax-TE with HepG2 cells cultured in Plasmax. Significantly differentially downregulated proteins whose transcripts were not significantly altered are highlighted in green. Significantly differentially upregulated proteins whose transcripts were not significantly altered are highlighted in magenta. Metalloproteins are highlighted in blue. (E) Heatmap of metalloprotein expression in HepG2 cells cultured in EMEM, Plasmax, Plasmax-TE or Plasmax-TE+Fe as determined by proteomic analysis, n=5. For all experiments, *P <0.05 , ns = not significant.

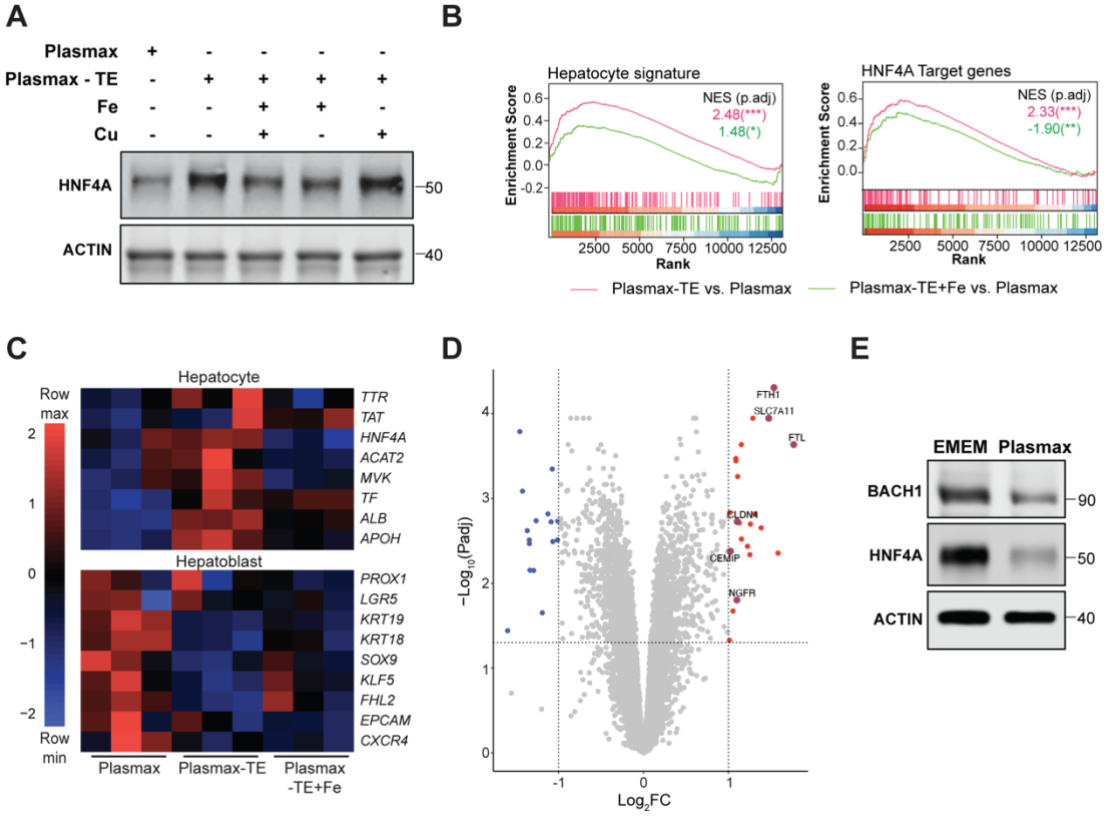

Figure 4. Iron availability contributes to the regulation of hepatocyte cell fate
(A) Representative immunoblot analysis of HepG2 cells cultured in Plasmax, Plasmax-TE, Plasmax-TE+Fe, Plasmax-TE supplemented with copper salts (0.005 μM cupric sulfate), or Plasmax-TE supplemented with iron and copper salts (0.12 μM ferric nitrate, 1.04 μM ferric sulfate, 0.005 μM cupric sulfate). (B) GSEA plots derived from RNA-Seq analysis comparing HepG2 cells cultured in Plasmax-TE with HepG2 cells cultured in Plasmax and comparing HepG2 cells cultured in Plasmax-TE+Fe with HepG2 cells cultured in Plasmax demonstrating signatures associated with hepatocyte cell state and function. (C) Heatmap of hepatocyte and hepatoblast gene expression in Plasmax, Plasmax-TE or Plasmax-TE+Fe as determined by RNA-Seq analysis, n=3. (D) Volcano plot of differentially expressed proteins identified from proteomic analysis comparing HepG2 cells cultured in Plasmax-TE+Fe with HepG2 cells cultured in Plasmax-TE, n=5. BACH1 targets are highlighted in maroon. Significantly upregulated proteins are highlighted in red. Significantly downregulated proteins are highlighted in blue. (E) Representative immunoblot analysis of HepG2 cells cultured in EMEM or Plasmax.

References

Addess KJ, Basilion JP, Klausner RD, Rouault TA & Pardi A (1997) Structure and dynamics of the iron responsive element RNA: implications for binding of the RNA by iron regulatory binding proteins. *J Mol Biol* 274: 72–83

Aden DP, Fogel A, Plotkin S, Damjanov I & Knowles BB (1979) Controlled synthesis of HBsAg in a differentiated human liver carcinoma-derived cell line. *Nature* 282: 615–616

Afgan E, Baker D, van den Beek M, Blankenberg D, Bouvier D, Čech M, Chilton J, Clements D, Coraor N, Eberhard C, *et al* (2016) The Galaxy platform for accessible, reproducible and collaborative biomedical analyses: 2016 update. *Nucleic Acids Res* 44: W3–W10

Ajioka RS, Phillips JD & Kushner JP (2006) Biosynthesis of heme in mammals. *Biochim Biophys Acta* 1763: 723–736

Apiz Saab JJ, Dzierozynski LN, Jonker PB, AminiTabrizi R, Shah H, Menjivar RE, Scott AJ, Nwosu ZC, Zhu Z, Chen RN, *et al* (2023) Pancreatic tumors exhibit myeloid-driven amino acid stress and upregulate arginine biosynthesis. *Elife* 12

Arzumanian VA, Kiseleva OI & Poverennaya EV (2021) The curious case of the HepG2 cell line: 40 years of expertise. *Int J Mol Sci* 22: 13135

Aziz N & Munro HN (1987) Iron regulates ferritin mRNA translation through a segment of its 5' untranslated region. *Proc Natl Acad Sci U S A* 84: 8478–8482

Biancur DE, Paulo JA, Małachowska B, Del Rey MQ, Sousa CM, Wang X, Sohn ASW, Chu GC, Gygi SP, Harper JW, *et al* (2017) Compensatory metabolic networks in pancreatic cancers upon perturbation of glutamine metabolism. *Nat Commun* 8: 15965

Boon R, Kumar M, Tricot T, Elia I, Ordovas L, Jacobs F, One J, De Smedt J, Eelen G, Bird M, *et al* (12/2020) Amino acid levels determine metabolism and CYP450 function of hepatocytes and hepatoma cell lines. *Nat Commun* 11: 1393

Cantor JR (2019) The rise of physiologic media. *Trends Cell Biol* 29: 854–861

Cantor JR, Abu-Remaileh M, Kanarek N, Freinkman E, Gao X, Louissaint A Jr, Lewis CA & Sabatini DM (2017) Physiologic medium rewires cellular metabolism and reveals uric acid as an endogenous inhibitor of UMP synthase. *Cell* 169: 258-272.e17

Chambers I, Frampton J, Goldfarb P, Affara N, McBain W & Harrison PR (1986) The structure of the mouse glutathione peroxidase gene: the selenocysteine in the active site is encoded by the "termination" codon, TGA. *EMBO J* 5: 1221–1227

Charafe-Jauffret E, Ginestier C, Monville F, Finetti P, Adélaïde J, Cervera N, Fekairi S, Xerri L, Jacquemier J, Birnbaum D, *et al* (2006) Gene expression profiling of breast cell lines identifies potential new basal markers. *Oncogene* 25: 2273–2284

Chen L, Zhang C, Xue R, Liu M, Bai J, Bao J, Wang Y, Jiang N, Li Z, Wang W, *et al* (2024) Deep whole-genome analysis of 494 hepatocellular carcinomas. *Nature* 627: 586–593

431 Chen Y, Guo X, Zeng Y, Mo X, Hong S, He H, Li J, Fatima S & Liu Q (2023) Oxidative stress
432 induces mitochondrial iron overload and ferroptotic cell death. *Sci Rep* 13: 15515

433 Copeland PR (2003) Regulation of gene expression by stop codon recoding: selenocysteine.
434 *Gene* 312: 17–25

435 Davidson SM, Papagiannakopoulos T, Olenchock BA, Heyman JE, Keibler MA, Luengo A,
436 Bauer MR, Jha AK, O'Brien JP, Pierce KA, *et al* (2016) Environment impacts the
437 metabolic dependencies of Ras-driven non-small cell lung cancer. *Cell Metab* 23:
438 517–528

439 Demichev V, Messner CB, Vernardis SI, Lilley KS & Ralser M (2020) DIA-NN: neural
440 networks and interference correction enable deep proteome coverage in high
441 throughput. *Nat Methods* 17: 41–44

442 Dulbecco R & Freeman G (1959) Plaque production by the polyoma virus. *Virology* 8: 396–
443 397

444 Eagle H (1959) Amino acid metabolism in mammalian cell cultures. *Science* 130: 432–437

445 Flickinger KM, Wilson KM, Rossiter NJ, Hunger AL, Vishwasrao PV, Lee TD, Mellado Fritz
446 CA, Richards RM, Hall MD & Cantor JR (2024) Conditional lethality profiling reveals
447 anticancer mechanisms of action and drug-nutrient interactions. *Sci Adv* 10:
448 eadq3591

449 Gordillo M, Evans T & Gouon-Evans V (2015) Orchestrating liver development.
450 *Development* 142: 2094–2108

451 Gray NK & Hentze MW (1994) Iron regulatory protein prevents binding of the 43S translation
452 pre-initiation complex to ferritin and eALAS mRNAs. *EMBO J* 13: 3882–3891

453 Hentze MW, Caughman SW, Rouault TA, Barriocanal JG, Dancis A, Harford JB & Klausner
454 RD (1987) Identification of the iron-responsive element for the translational regulation
455 of human ferritin mRNA. *Science* 238: 1570–1573

456 Jiang X, Liu K, Jiang H, Yin H, Wang E-D, Cheng H, Yuan F, Xiao F, Wang F, Lu W, *et al*
457 (2023) SLC7A14 imports GABA to lysosomes and impairs hepatic insulin sensitivity
458 via inhibiting mTORC2. *Cell Rep* 42: 111984

459 Kao Y-R, Chen J, Kumari R, Ng A, Zintiridou A, Tatiparthy M, Ma Y, Aivalioti MM, Moulik D,
460 Sundaravel S, *et al* (2024) An iron rheostat controls hematopoietic stem cell fate. *Cell*
461 *Stem Cell* 31: 378-397.e12

462 Katsuda T, Sussman JH, Ito K, Katznelson A, Yuan S, Takenaka N, Li J, Merrell AJ, Cure H,
463 Li Q, *et al* (2024) Cellular reprogramming in vivo initiated by SOX4 pioneer factor
464 activity. *Nat Commun* 15: 1761

465 Kaur S, Kidambi S, Ortega-Ribera M, Thuy LTT, Nieto N, Cogger VC, Xie W-F, Tacke F &
466 Gracia-Sancho J (2023) In vitro models for the study of liver biology and diseases:
467 Advances and limitations. *Cell Mol Gastroenterol Hepatol* 15: 559–571

468 Kitamuro T, Takahashi K, Ogawa K, Udono-Fujimori R, Takeda K, Furuyama K, Nakayama
469 M, Sun J, Fujita H, Hida W, *et al* (2003) Bach1 functions as a hypoxia-inducible
470 repressor for the heme oxygenase-1 gene in human cells. *J Biol Chem* 278: 9125–
471 9133

472 Kolde R (2012) Pheatmap: pretty heatmaps. *R package version*

473 Kryukov GV, Castellano S, Novoselov SV, Lobanov AV, Zehtab O, Guigó R & Gladyshev VN
474 (2003) Characterization of mammalian selenoproteomes. *Science* 300: 1439–1443

475 Lagziel S, Gottlieb E & Shlomi T (2020) Mind your media. *Nature Metabolism*: 1–4

476 Law CW, Chen Y, Shi W & Smyth GK (2014) voom: Precision weights unlock linear model
477 analysis tools for RNA-seq read counts. *Genome Biol* 15: R29

478 Lignitto L, LeBoeuf SE, Homer H, Jiang S, Askenazi M, Karakousi TR, Pass HI, Bhutkar AJ,
479 Tsirigos A, Ueberheide B, *et al* (2019) Nrf2 Activation Promotes Lung Cancer
480 Metastasis by Inhibiting the Degradation of Bach1. *Cell* 178: 316-329.e18

481 Lin C-Y, Chang T-W, Hsieh W-H, Hung M-C, Lin I-H, Lai S-C & Tzeng Y-J (2016)
482 Simultaneous induction of apoptosis and necroptosis by Tanshinone IIA in human
483 hepatocellular carcinoma HepG2 cells. *Cell Death Discov* 2: 16065

484 Liu F, Tian T, Zhang Z, Xie S, Yang J, Zhu L, Wang W, Shi C, Sang L, Guo K, *et al* (2022)
485 Long non-coding RNA SNHG6 couples cholesterol sensing with mTORC1 activation
486 in hepatocellular carcinoma. *Nat Metab* 4: 1022–1040

487 Liu Z, Xu Y, Zhang W, Gao X, Luo G, Song H, Liu J & Wang H (2021) Identification of targets
488 of JS-K against HBV-positive human hepatocellular carcinoma HepG2.2.15 cells with
489 iTRAQ proteomics. *Sci Rep* 11: 10381

490 López-Terrada D, Cheung SW, Finegold MJ & Knowles BB (2009) Hep G2 is a
491 hepatoblastoma-derived cell line. *Hum Pathol* 40: 1512–1515

492 Muir A, Danai LV, Gui DY, Waingarten CY, Lewis CA & Vander Heiden MG (2017)
493 Environmental cystine drives glutamine anaplerosis and sensitizes cancer cells to
494 glutaminase inhibition. *Elife* 6: e27713

495 Muir A & Vander Heiden MG (2018) The nutrient environment affects therapy. *Science* 360:
496 962–963

497 Müller S, Sindikubwabo F, Cañeque T, Lafon A, Versini A, Lombard B, Loew D, Wu T-D,
498 Ginestier C, Charafe-Jauffret E, *et al* (2020) CD44 regulates epigenetic plasticity by
499 mediating iron endocytosis. *Nat Chem* 12: 929–938

500 Neve RM, Chin K, Fridlyand J, Yeh J, Baehner FL, Fevr T, Clark L, Bayani N, Coppe J-P,
501 Tong F, *et al* (2006) A collection of breast cancer cell lines for the study of functionally
502 distinct cancer subtypes. *Cancer Cell* 10: 515–527

503 Ogawa K, Sun J, Taketani S, Nakajima O, Nishitani C, Sassa S, Hayashi N, Yamamoto M,
504 Shibahara S, Fujita H, *et al* (2001) Heme mediates derepression of Maf recognition
505 element through direct binding to transcription repressor Bach1. *EMBO J* 20: 2835–
506 2843

507 Ong AJS, Bladen CE, Tigani TA, Karamalakis AP, Evason KJ, Brown KK & Cox AG (2023)
508 The KEAP1-NRF2 pathway regulates TFEB/TFE3-dependent lysosomal biogenesis.
509 *Proc Natl Acad Sci U S A* 120: e2217425120

510 Oyake T, Itoh K, Motohashi H, Hayashi N, Hoshino H, Nishizawa M, Yamamoto M & Igarashi
511 K (1996) Bach proteins belong to a novel family of BTB-basic leucine zipper

transcription factors that interact with MafK and regulate transcription through the NF-E2 site. *Mol Cell Biol* 16: 6083–6095

Park S, Park J-H, Jung H-J, Jang J-H, Ahn S, Kim Y, Suh P-G, Chae S, Yoon JH, Ryu SH, *et al* (2018) A secretome profile indicative of oleate-induced proliferation of HepG2 hepatocellular carcinoma cells. *Exp Mol Med* 50: 1–14

Parviz F, Matullo C, Garrison WD, Savatski L, Adamson JW, Ning G, Kaestner KH, Rossi JM, Zaret KS & Duncan SA (2003) Hepatocyte nuclear factor 4alpha controls the development of a hepatic epithelium and liver morphogenesis. *Nat Genet* 34: 292–296

Pyun J, McInnes LE, Donnelly PS, Mawal C, Bush AI, Short JL & Nicolazzo JA (2022) Copper bis(thiosemicarbazone) complexes modulate P-glycoprotein expression and function in human brain microvascular endothelial cells. *J Neurochem* 162: 226–244

Rao X, Huang X, Zhou Z & Lin X (2013) An improvement of the 2ˆ(-delta delta CT) method for quantitative real-time polymerase chain reaction data analysis. *Biostat Bioinform Biomath* 3: 71–85

Rawat V, DeLear P, Prashanth P, Ozgurses ME, Tebeje A, Burns PA, Conger KO, Solís C, Hasnain Y, Novikova A, *et al* (2024) Drug screening in human physiologic medium identifies uric acid as an inhibitor of rigosertib efficacy. *JCI Insight* 9

Rossiter NJ, Huggler KS, Adelmann CH, Keys HR, Soens RW, Sabatini DM & Cantor JR (2021) CRISPR screens in physiologic medium reveal conditionally essential genes in human cells. *Cell Metab* 33: 1248-1263.e9

Sanghvi VR, Leibold J, Mina M, Mohan P, Berishaj M, Li Z, Miele MM, Lailler N, Zhao C, de Stanchina E, *et al* (2019) The Oncogenic Action of NRF2 Depends on De-glycation by Fructosamine-3-Kinase. *Cell* 178: 807-819.e21

Sekiya S & Suzuki A (2011) Direct conversion of mouse fibroblasts to hepatocyte-like cells by defined factors. *Nature* 475: 390–393

Senkowski W, Gall-Mas L, Falco MM, Li Y, Lavikka K, Kriegbaum MC, Oikkonen J, Bulanova D, Pietras EJ, Voßgröne K, *et al* (2023) A platform for efficient establishment and drug-response profiling of high-grade serous ovarian cancer organoids. *Dev Cell* 58: 1106-1121.e7

Shen M, Goforth JB & Eisenstein RS (2023) Iron-dependent post transcriptional control of mitochondrial aconitase expression. *Metallomics* 15

Smyth GK (2005) limma: Linear Models for Microarray Data. In *Bioinformatics and Computational Biology Solutions Using R and Bioconductor* pp 397–420. New York: Springer-Verlag

Sun J, Hoshino H, Takaku K, Nakajima O, Muto A, Suzuki H, Tashiro S, Takahashi S, Shibahara S, Alam J, *et al* (2002) Hemoprotein Bach1 regulates enhancer availability of heme oxygenase-1 gene. *EMBO J* 21: 5216–5224

Tardito S, Oudin A, Ahmed SU, Fack F, Keunen O, Zheng L, Miletic H, Sakariassen PØ, Weinstock A, Wagner A, *et al* (2015) Glutamine synthetase activity fuels nucleotide biosynthesis and supports growth of glutamine-restricted glioblastoma. *Nat Cell Biol* 17: 1556–1568

554 Vande Voorde J, Ackermann T, Pfetzer N, Sumpton D, Mackay G, Kalna G, Nixon C, Blyth K,
555 Gottlieb E & Tardito S (2019) Improving the metabolic fidelity of cancer models with a
556 physiological cell culture medium. *Sci Adv* 5: eaau7314

557 Wei X, Guo J, Li Q, Jia Q, Jing Q, Li Y, Zhou B, Chen J, Gao S, Zhang X, *et al* (2019) Bach1
558 regulates self-renewal and impedes mesendodermal differentiation of human
559 embryonic stem cells. *Sci Adv* 5: eaau7887

560 Wickham H (2016) ggplot2: Elegant Graphics for Data Analysis Cham: Springer International
561 Publishing

562 Wiel C, Le Gal K, Ibrahim MX, Jahangir CA, Kashif M, Yao H, Ziegler DV, Xu X, Ghosh T,
563 Mondal T, *et al* (2019) BACH1 Stabilization by Antioxidants Stimulates Lung Cancer
564 Metastasis. *Cell* 178: 330-345.e22

565 Yang S, Ooka M, Margolis RJ & Xia M (2023) Liver three-dimensional cellular models for
566 high-throughput chemical testing. *Cell Rep Methods* 3: 100432

567 Yu G, Wang L-G, Han Y & He Q-Y (2012) clusterProfiler: an R package for comparing
568 biological themes among gene clusters. *OMICS* 16: 284–287

569 Zhang Z-L, Liu G-C, Peng L, Zhang C, Jia Y-M, Yang W-H & Mao L (2018) Effect of PAK1
570 gene silencing on proliferation and apoptosis in hepatocellular carcinoma cell lines
571 MHCC97-H and HepG2 and cells in xenograft tumor. *Gene Ther* 25: 284–296

572 Zhuang X, Wang Q, Joost S, Ferrena A, Humphreys DT, Li Z, Blum M, Krause K, Ding S,
573 Landais Y, *et al* (2025) Ageing limits stemness and tumorigenesis by reprogramming
574 iron homeostasis. *Nature* 637: 184–194

575 Zinoni F, Birkmann A, Stadtman TC & Böck A (1986) Nucleotide sequence and expression of
576 the selenocysteine-containing polypeptide of formate dehydrogenase (formate-
577 hydrogen-lyase-linked) from Escherichia coli. *Proc Natl Acad Sci U S A* 83: 4650–
578 4654